Published in J. Comput. Phys. 216 (2006), no. 2, 573–588

A NEW ALGORITHM FOR TOPOLOGY OPTIMIZATION USING A LEVEL-SET METHOD

SAMUEL AMSTUTZ AND HEIKO ANDRÄ

Abstract. The level-set method has been recently introduced in the field of shape optimization, enabling a smooth representation of the boundaries on a fixed mesh and therefore leading to fast numerical algorithms. However, most of these algorithms use a Hamilton-Jacobi equation to connect the evolution of the level-set function with the deformation of the contours, and consequently they can hardly create new holes in the domain (at least in 2D). In this work, we propose an evolution equation for the level-set function based on a generalization of the concept of topological gradient. This results in a new algorithm allowing for all kinds of topology changes.

1. Introduction

Many methods have been worked out for the automatic optimization of elastic structures. The oldest and most popular one, the so-called classical shape optimization method [21, 28], is based on the computation of the sensitivity of the criterion of interest with respect to a smooth variation of the boundary. Its main drawback is that it does not allow any topology changes. To overcome this limitation, relaxed formulations using *e.g.* the homogenization theory have been introduced [1, 2, 6, 11, 12, 18]. However, these methods are mainly restricted to linear elasticity and particular objective functions. Despite their high computational cost, stochastic algorithms (like genetic algorithms, see *e.g.* [19]) can be used to deal with more general situations, or when practical reasons make difficult a sensitivity computation (for instance the adjoint state may not be easily computable).

The level-set method, which has several advantages, was instigated by Osher and Sethian [23] for numerically tracking fronts and free boundaries, and recently introduced in the field of shape optimization [4, 5, 13, 22, 25, 30]. First, its main feature is to enable an accurate description of the boundaries on a fixed mesh. Therefore it leads to fast numerical algorithms. Second, its range of application is very wide, since the front velocity can be derived from the classical shape sensitivity. Finally, it can handle some topology changes. Indeed, within the usual framework of the control of the level-set function by a Hamilton-Jacobi equation, the merging and cancellation of holes prove to occur in a natural way. Conversely, the nucleation of new holes seems to be rather unlikely in practical situations. In 3D, holes can still appear by pinching two boundaries, but this process is impossible in 2D. It follows that the obtained design is strongly dependent on the initial guess in this case.

Besides, the notion of topological gradient [16, 20, 24, 27] has been devised to measure the sensitivity of a criterion with respect to the size of a small hole created around a given point of the domain. This concept gave rise to another class of optimal design algorithms. In structural optimization, one usually uses a fixed point method of the type

$$\Omega_{k+1} := \{x \in \Omega_k, g_k(x) > c_k\}, \quad k = 0, 1, 2, \dots, \tag{1}$$

where g_k denotes the topological gradient computed in the domain Ω_k and $c_k < 0$ is a threshold playing the role of a step size (see [16, 15]). The main drawback of this procedure is its inability to add matter in some places where it has been removed "by mistake" at previous iterations.

In this paper, we propose a modification of (1) based on a generalization of the concept of topological gradient and the representation of the domain by a level-set function possibly

different from this quantity. This results in a new algorithm allowing for all kinds of topology changes. Its convergence to a (local) minimum is illustrated by several numerical experiments performed in the contexts of structural mechanics and porous medium flows. Unlike other algorithms which have been developed on the same purpose [3, 14, 31], we have completely abandoned the Hamilton-Jacobi equation, getting quite far from the usual notion of "level-set method".

2. Presentation of a model problem

Let D be a smooth domain of $\mathbb{R}^d$ ($d = 2$ or 3) and Ω be a smooth subdomain of D occupied by a linear isotropic elastic material. The latter stands for the design domain, *i.e.* the domain we want to optimize, whereas the former is a fixed set meant to define the maximum bulk of the structure as well as to serve as a computational box. The boundary ∂D of D is made of the three disjoint parts

$$\partial D = \Gamma_D \cup \Gamma_F \cup \Gamma_N,$$

with Γ_D of nonzero Lebesgue measure. We assume that the boundary of Ω satisfies

$$\partial\Omega = (\Gamma_D \cap \partial\Omega) \cup \Gamma_F \cup (\Gamma_N \cap \partial\Omega) \cup \Gamma_0,$$

where $\Gamma_0 = \partial\Omega \cap D$ (see Fig. 1). For a given load $\varphi \in (H^{-1/2}(\Gamma_F))^d$, the mixed boundary value problem (b.v.p.) for the displacement u_Ω reads as follows in linear elasticity:

$$\left\{\begin{array}{rcll} -\mathrm{div}\,(Ae(u_\Omega)) &=& 0 & \text{in} \quad \Omega, \\ u_\Omega &=& 0 & \text{on} \quad \Gamma_D \cap \partial\Omega, \\ (Ae(u_\Omega))n &=& \varphi & \text{on} \quad \Gamma_F, \\ (Ae(u_\Omega))n &=& 0 & \text{on} \quad (\Gamma_N \cap \partial\Omega) \cup \Gamma_0. \end{array}\right. \tag{2}$$

In this system, A denotes the Hooke's tensor of the material and $e(u_\Omega)$ denotes the linearized strain tensor. Note that the part Γ_F of the border where the load is applied is prescribed.

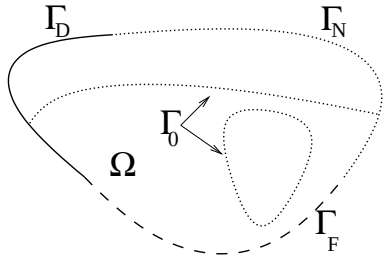

Figure 1. The working domain D.

To fix ideas, we consider a criterion $j(\Omega)$ made of the compliance complemented with a term accounting for the weight of the structure, *i.e.*

$$j(\Omega) = J(u_\Omega) + \ell|\Omega|, \tag{3}$$

where the functional J is defined on $(H^1(\Omega))^d$ by

$$J(u) = \int_{\Gamma_F} \varphi.u ds \tag{4}$$

and $|\Omega|$ is the Lebesgue measure of Ω. The constant $\ell > 0$ is given and can be interpreted as a Lagrange multiplier. Due to the Green's formula, the compliance can also be computed by

$$J(u_\Omega) = \int_\Omega Ae(u_\Omega) : e(u_\Omega) dx. \tag{5}$$

However, we will prefer the formulation (4) which turns out to be more convenient from the numerical point of view. We are interested in the topological shape optimization problem

$$\inf_{\Omega \in \mathcal{U}_{ad}} j(\Omega),$$

with

$$\mathcal{U}_{ad} = \{\Omega \subset D, \Gamma_F \subset \partial\Omega, \text{meas } (\Gamma_D \cap \partial\Omega) \neq 0\}.$$

By (5) and the Korn's inequality, $j(\Omega) \geq 0$ and the above infimum exists in $\mathbb{R}_+$, but it is generally not attained in this set of admissible domains. Nevertheless, the algorithm we will present only requires the existence of a local minimum.

To avoid remeshing, the elasticity problem (2) is approximated for $\varepsilon \to 0$ by the following b.v.p. with variable coefficients, formulated in the fixed domain D:

$$\left\{ \begin{array}{rcll} -\text{div } (\tilde{\alpha} A e(u_\Omega)) & = & 0 & \text{in } D, \\ u_\Omega & = & 0 & \text{on } \Gamma_D, \\ (Ae(u_\Omega))n & = & \varphi & \text{on } \Gamma_F, \\ (Ae(u_\Omega))n & = & 0 & \text{on } \Gamma_N, \end{array} \right. \tag{6}$$

with

$$\tilde{\alpha} = \left\{ \begin{array}{ll} 1 & \text{in } \Omega, \\ \varepsilon & \text{in } D \setminus \overline{\Omega}. \end{array} \right. \tag{7}$$

The constant ε must be chosen small enough to mimic Problem (2) with a suitable accuracy. In the computations presented in Sections 4 and 5, a fixed value $\varepsilon = 10^{-3}$ has been used.

3. Description of the algorithm

3.1. **Topological sensitivity.** At a point $x \in \Omega$, the topological gradient $g(x)$ is a number that measures the sensitivity of the criterion $j(\Omega)$ with respect to the creation of a small hole around x. More precisely, it is defined by the topological asymptotic expansion

$$j(\Omega \setminus \overline{B(x,\rho)}) - j(\Omega) = f(\rho)g(x) + o(f(\rho)), \tag{8}$$

where $B(x,\rho)$ is the ball of center x and radius ρ and $f(\rho)$ is a smooth positive function going to zero with ρ. In this work, only circular or spherical holes are considered although such an expansion can be obtained for arbitrary shaped holes and also for cracks.

Actually, in our algorithm, it is interesting to consider not the creation of a real hole but the insertion of the soft material we have introduced to simulate void. As expected, the comparison of the corresponding asymptotic expansions shows that the sensitivities with respect to both kinds of perturbation tend to be identical when the density ε tends to zero. However, the advantage of this approach is that it allows for the opposite operation, *i.e.* to strengthen the weak phase.

In [8], the asymptotic expansion (8) has been generalized to the case where the density $\tilde{\alpha}$ inside the ball $B(x,\rho)$ is shifted from its initial value α_0 into the new value α_1. By using the expression of the elastic moment tensor calculated in [7], the following functions have been obtained in linear elasticity 2D plane strain:

$$\left\{ \begin{array}{l} f(\rho) = |B(x,\rho)|, \\ g(x) = \dfrac{r-1}{\kappa r+1}\dfrac{\kappa+1}{2}\left[2\sigma(u_\Omega) : e(v_\Omega) + \dfrac{(r-1)(\kappa-2)}{\kappa+2r-1}\text{tr}\sigma(u_\Omega)\text{tr}e(v_\Omega)\right] + \ell\delta, \end{array} \right.$$

with

$$r = \frac{\alpha_1}{\alpha_0}, \qquad \kappa = \frac{\lambda+3\mu}{\lambda+\mu}.$$

The constants λ and μ are the Lamé coefficients and the stress tensor $\sigma(u_\Omega)$ is computed with the local density at the point x. In plane stress, $\lambda^* = 2\mu\lambda/(\lambda+2\mu)$ must be substituted for

λ. The displacement field v_Ω is the adjoint state and the binary variable δ is introduced for convenience to indicate the sense of the variation of surface of Ω:

$$\delta = \begin{cases} -1 & \text{if } |\Omega| \text{ is decreased (creation of a hole),} \\ +1 & \text{if } |\Omega| \text{ is increased (addition of matter).} \end{cases} \tag{9}$$

For the cost functional (4), the problem is well-known to be self-adjoint, *i.e.* $v_\Omega = -u_\Omega$.

In our case, α_0 and α_1 can only take the values 1 and ε. When $\alpha_0 = 1$, the only perturbation possible is the creation of a hole, which means that $\alpha_1 = \varepsilon$, $r = \varepsilon$ and $\delta = -1$. The associated gradient is

$$g_-(x) = \frac{\varepsilon - 1}{\kappa\varepsilon + 1}\frac{\kappa + 1}{2}\left[2\sigma(u_\Omega) : e(v_\Omega) + \frac{(\varepsilon - 1)(\kappa - 2)}{\kappa + 2\varepsilon - 1}\mathrm{tr}\sigma(u_\Omega)\mathrm{tr}e(v_\Omega)\right] - \ell.$$

When $\alpha_0 = \varepsilon$, we have to consider a reinforcement, *i.e.* $\alpha_1 = 1$, $r = 1/\varepsilon$ and $\delta = +1$. The associated gradient is

$$g_+(x) = \frac{1 - \varepsilon}{\kappa + \varepsilon}\frac{\kappa + 1}{2}\left[2\sigma(u_\Omega) : e(v_\Omega) + \frac{(1 - \varepsilon)(\kappa - 2)}{\kappa\varepsilon + 2 - \varepsilon}\mathrm{tr}\sigma(u_\Omega)\mathrm{tr}e(v_\Omega)\right] + \ell.$$

As said before, g_- as well as g_+ can be accurately computed by taking $\varepsilon = 0$ in the above expressions. We define the quantity

$$\tilde{g}(x) = \begin{cases} -g_-(x) & \text{if} \quad x \in \Omega, \\ g_+(x) & \text{if} \quad x \in D \setminus \overline{\Omega} \end{cases} \tag{10}$$

that measures the sensitivity of the criterion $j(\Omega)$ with respect to an oriented shift of the density. It follows that a necessary local minimality condition for the approximated problem (6) is

$$\begin{cases} \tilde{g}(x) & \leq & 0 & \text{in} & \Omega, \\ \tilde{g}(x) & \geq & 0 & \text{in} & D \setminus \overline{\Omega}, \end{cases} \tag{11}$$

and that a sufficient local minimality condition for this class of domain perturbations is

$$\begin{cases} \tilde{g}(x) & < & 0 & \text{in} & \Omega, \\ \tilde{g}(x) & > & 0 & \text{in} & D \setminus \overline{\Omega}. \end{cases} \tag{12}$$

3.2. **Representation by a level-set function.** As it is common in level-set methods, we introduce a fictitious time t and we consider a family of domains $(\Omega(t))_{t\geq 0}$. This family is represented by a level-set function $\psi : \mathbb{R} \times D \to \mathbb{R}$ such that

$$\begin{cases} \psi(t,x) & < & 0 & \Longleftrightarrow & x \in \Omega(t), \\ \psi(t,x) & > & 0 & \Longleftrightarrow & x \in D \setminus \overline{\Omega(t)}, \\ \psi(t,x) & = & 0 & \Longleftrightarrow & x \in \Gamma_0(t). \end{cases} \tag{13}$$

For our topological shape optimization problem, we choose ψ as a design variable. We denote by $\tilde{g}(t,x)$ the generalized topological gradient associated to the domain $\Omega(t)$ and computed at the point x. Our algorithm is motivated by the following remarks.

(1) In the domain $\Omega(t)$, one would like to increase the level-set function (in order to push it in the direction where holes appear) where $g_- < 0$, *i.e.* $\tilde{g} > 0$. Conversely, in $D \setminus \Omega(t)$, one would like to decrease the level-set function where $g_+ < 0$, *i.e.* $\tilde{g} < 0$. Thus a natural algorithm would be to control the level-set function by the differential equation

$$\frac{\partial \psi}{\partial t} = \tilde{g}.$$

Unfortunately, since $\tilde{g}$ is not bound to vanish at an optimum, this algorithm will generally diverge.

(2) The level-set function represents the same domain when it is multiplied by a positive constant. Therefore it may be beneficial for the stability of the algorithm to get rid of this useless degree of freedom by imposing *e.g.* that a certain norm of the level-set function is preserved.

(3) At a (local) minimum of the objective function, if the optimality conditions (12) are satisfied, then the generalized topological gradient can be used as a level-set function to represent the corresponding domain.

Therefore, instead of governing the evolution in time of the level-set function by a Hamilton-Jacobi equation propagating the interface $\Gamma_0(t)$, we propose the equations

$$\psi(0,.) \in \mathcal{S}, \tag{14}$$

$$\frac{\partial \psi}{\partial t} = P_{\psi^\perp}(\tilde{g}) \qquad \forall t \geq 0, \tag{15}$$

where $P_{\psi^\perp}$ is the orthogonal projector onto the orthogonal complement of ψ, *i.e.*

$$P_{\psi^\perp}(\tilde{g}) = \tilde{g} - \frac{(\tilde{g},\psi)}{\|\psi\|^2}\psi.$$

In the above relations, the inner product $(.,.)$, the norm $\|.\|$ as well as the unit sphere $\mathcal{S}$ refer to the Hilbert space $L^2(D)$. This choice will be explained later on. The solution of (14), (15) satisfies the following outstanding properties.

(1) It comes straightforwardly (*i.e.* by multiplying both sides of Equation (15) in the sense of the inner product by ψ) that

$$\psi(t,.) \in \mathcal{S} \qquad \forall t \geq 0.$$

(2) If ψ tends to a stationary point and if the topological gradient $\tilde{g}$ at that point is nonzero, then it is a local optimum of the topological shape optimization problem. Indeed, the relation $P_{\psi^\perp}(\tilde{g}) = 0$ implies the existence of a real number s such that $\tilde{g} = s\psi$. If $s > 0$, then the conditions (12) are fulfilled and we are in the presence of a local minimum. If $s < 0$, then a local maximum has been reached. However this latter situation is highly unlikely since the algorithm is constructed in order to decrease the criterion.

3.3. **Numerical algorithm.** Let us first focus on the time discretization. We consider a sequence $(t_i)_{i\in\mathbb{N}}$ such that the variation of the topological gradient can be neglected in the interval $[t_i, t_{i+1}]$. In this way, (15) can be solved analytically in the interval $[t_i, t_{i+1}]$ (Euler's scheme on the sphere): there exists an angle $\xi_i \in [0, \theta_i]$ such that

$$\psi_{i+1} = \cos\xi_i.\psi_i + \sin\xi_i.\frac{P_{\psi_i^\perp}(\tilde{g}_i)}{\|P_{\psi_i^\perp}(\tilde{g}_i)\|}. \tag{16}$$

The notations $\psi_i(x) = \psi(t_i, x)$ and $\tilde{g}_i(x) = \tilde{g}(t_i, x)$ are used, and θ_i is the non-oriented angle between the vectors ψ_i and $\tilde{g}_i$, *i.e.*

$$\theta_i = \arccos\frac{(\psi_i, \tilde{g}_i)}{\|\tilde{g}_i\|}.$$

For numerical purposes, we have interest to make the change of variable

$$\xi_i = \kappa_i\theta_i, \qquad \kappa_i \in [0,1].$$

By using trigonometric formulas we arrive easily at the relation

$$\psi_{i+1} = \frac{1}{\sin\theta_i}\left[\sin((1-\kappa_i)\theta_i).\psi_i + \sin(\kappa_i\theta_i).\frac{\tilde{g}_i}{\|\tilde{g}_i\|}\right]. \tag{17}$$

In this expression, the time has disappeared and κ_i plays the role of step size. Like in most optimization methods, this step size ought to be chosen in an adaptive way, in that we do not know a priori to which extent the sensitivity (here the topological gradient, which by definition is a local indicator) can be trusted. Since the evaluation of the objective function may be very costly from a computational point of view, a precise line search for the optimal step is generally inappropriate. We adopt the technique of [5] consisting merely in reducing the step if the criterion increases. Therefore, it is important to check that the level-set function is somehow

evolving along a descent direction. This is the goal of the following discussion. Consider that, for a sufficiently small value of κ_i, the computation of ψ_{i+1} by (17) leads to the creation of a small hole around a point $\tilde{x} \in \Omega_i$. So we have $\psi_i(\tilde{x}) < 0$ and $\psi_{i+1}(\tilde{x}) > 0$. From (17) it comes straightforwardly that $\tilde{g}_i(\tilde{x}) > 0$ (we recall that $\theta_i \in [0, \pi]$), which means that $g_i^-(\tilde{x}) < 0$. In the same way we obtain that an addition of matter around some point $\tilde{x} \in D \setminus \overline{\Omega_i}$ can only occur if $g_i^+(\tilde{x}) < 0$. In both cases the criterion should decrease.

Let us now discuss the spatial discretization. Let $\mathcal{U}_h$ be a finite dimensional subspace of $L^2(D)$, endowed with the induced inner product of $L^2(D)$. The design variable of the discretized problem is a level-set function ψ living in the unit ball $\mathcal{S}_h$ of $\mathcal{U}_h$. However, it is very important for the smoothness of the shape that the level-set function is continuous across the interface $\partial\Omega_i$. For this reason we construct $\mathcal{U}_h$ with the help of P_1 finite elements. Of course, higher order finite elements would also be possible. From the observation that, on the one hand, the numerical resolution of (6) is predominant in the global computational cost and, on the other hand, instabilities may occur if the solution has less degrees of freedom than the level-set function, we use the same mesh and the same finite elements for solving the PDE as for describing the level-set function. In the cells that are crossed by the curve of equation $\psi = 0$, the density $\tilde{\alpha}$ in (6) is computed by linear interpolation. The resulting topological gradient is interpolated the other way round, *i.e.* from the centers of the cells to the nodes, so that we get out a function $\tilde{g} \in \mathcal{U}_h$. Beyond the technical aspects of the implementation, this smoothing of the topological gradient is necessary because the exact function defined by (10) may have a jump across the boundary, which is very undesirable from the point of view of the evolution of the interface and would lead to a discontinuous level-set function after convergence. Nevertheless, its variation remains sharp, which justifies the use of the L^2 scalar product for the projection. Furthermore, let us recall that such a filtering of the sensitivity has been widely adopted in shape and topology optimization (see *e.g.* [26, 9]) because of its regularizing effect. This latter effect is particularly appreciated in topology optimization algorithms allowing nucleations which, to the best of our knowledge, are all unable to handle a perimeter penalization.

From the remarks above, we propose the following algorithm. For notational simplicity, all indexes h referring to a finite element approximation are omitted.

(1) Choose an initial level-set function $\psi_0 \in \mathcal{S}$ and an initial step κ_0.
(2) Iterate until target is reached:
   - construct the domain Ω_i by (13),
   - solve the elasticity problem (6) and compute the topological gradient $\tilde{g}_i$ by (10),
   - update the level-set function by (17) with a step κ_i chosen according to the previous iteration and possibly decreased until the criterion decreases.

In order to reduce the computational cost and, in the same time, to improve the robustness with respect to local minima, we have observed that it is generally beneficial to split the optimization process in several stages associated to different levels of accuracy. In this framework we start with a fairly coarse mesh and, after convergence (*i.e.* the design does not evolve any more), this mesh is refined, the level-set function is projected onto this new mesh and the optimization is restarted in this new configuration. This procedure is iterated until the desired accuracy is reached. In our computations, we performed simply a uniform mesh refinement although some kind of adaptivity might be profitable (see *e.g.* [29]).

The following section is devoted to the validation of the algorithm on classical examples. A more complex problem is addressed in Section 5.

4. Numerical examples in linear elasticity

4.1. **Cantilever.** The first example is the long cantilever problem that has been treated *e.g.* in [5, 3]. The computational box D is a rectangle of size 2×1 with an homogeneous Dirichlet condition on the left side and a vertical pointwise unitary load applied at the middle of the right side (see Fig. 2). To enable the comparison with the results obtained in [5, 3], we have taken

the same value $\ell = 100$ and a material with the same elastic parameters, namely the Young's modulus $E = 1$ and the Poisson's ratio $\nu = 0.3$. We present four computations.

In the first case the level-set function is initialized by the constant $\psi(0, x) = -1/\sqrt{|D|}$. Thus the initial domain Ω_0 is the whole box D. A mesh consisting of 4193 nodes is used during the whole optimization process. It is built so as to preserve the symmetry of the problem, otherwise little dissymmetries may occur (see the examples of Sections 4.4 and 5). The obtained design is represented in Figure 3. In the second case, we start with a coarse mesh (1073 nodes). After convergence (iteration 13), this mesh is uniformely refined, so that we obtain the same mesh as in the first case, and the optimization is pursued on this mesh. Figure 4 shows the designs obtained at the end of each stage. Figure 5 shows the corresponding level-set functions. In the other two cases, Ω_0 is an half-width horizontal strip (see Fig. 6) and ψ_0 is a negative constant inside this strip, a positive constant outside. Again, we present the results of computations preformed on a single mesh and on two consecutive meshes (Fig. 7). Comparative convergence histories of the criterion $j(\Omega_i)$ and of the angle θ_i are illustrated in Figure 8. The CPU times needed for those computation on a Intel Dual Xeon processor at 2.8 GHz are reported in Table 1.

FIGURE 2. Boundary conditions for the cantilever.

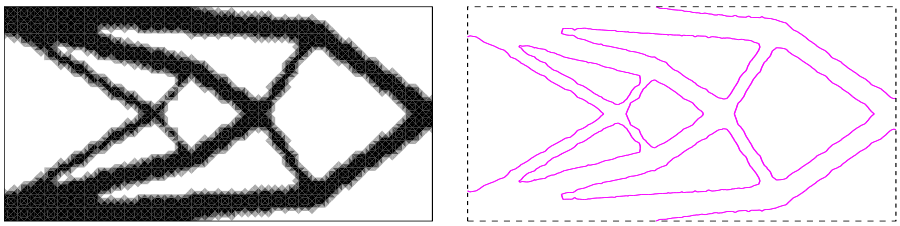

FIGURE 3. Iteration 25 of the cantilever with full domain initialization, the whole optimization being performed on a single mesh: material density (left) and iso-value zero of the level-set function (right).

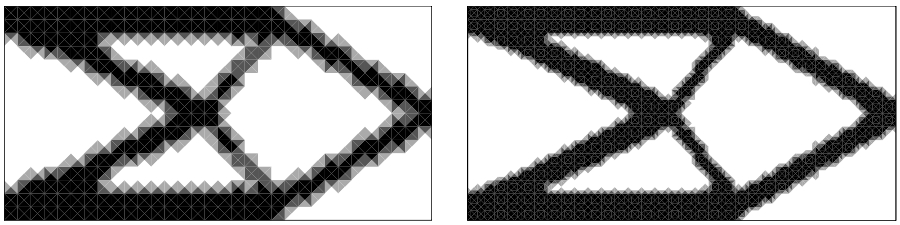

FIGURE 4. Iteration 13 (coarse mesh, last iteration before refinement) and 19 of the cantilever with full domain initialization.

Here are a few remarks concluding this first series of computations. First, the criterion is monotonically decreasing, this property being enforced by the algorithm, except after a mesh refinement where it may slightly increase. Second, θ_i does not tend exactly to zero because of

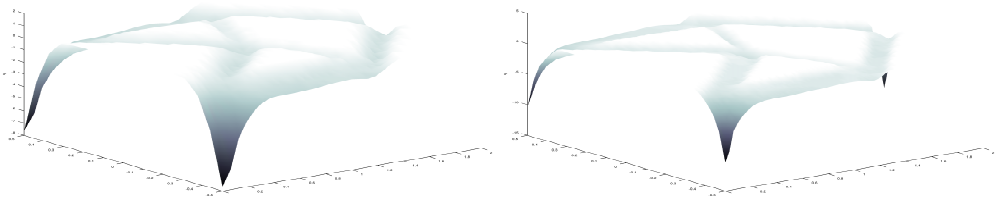

FIGURE 5. Level-set function corresponding to the designs of Fig. 4.

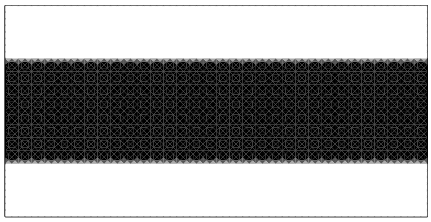

FIGURE 6. Half-width initialization.

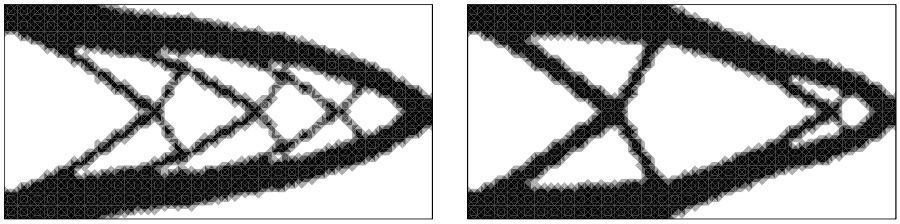

FIGURE 7. Iterations 38 (one stage) and 37 (two stages) of the cantilever initialized as in Fig. 6.

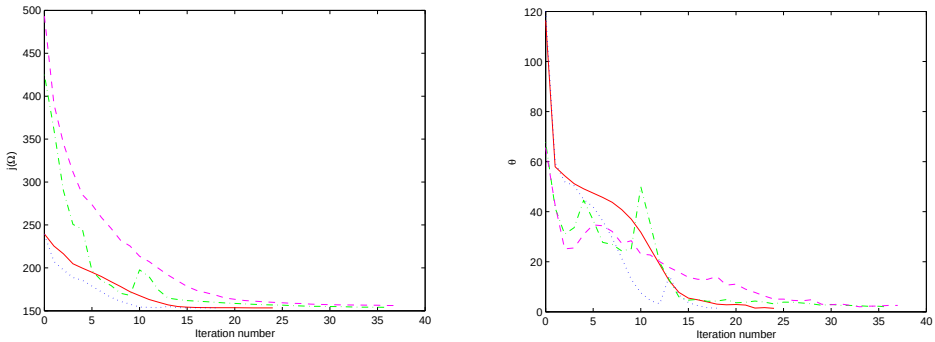

FIGURE 8. Convergence histories of the criterion $j(\Omega)$ (left) and of the angle θ expressed in degrees (right), for the examples of Fig. 3, 4 and 7 represented by a solid, dotted, dashed and dash-dotted line, respectively.

Case	1	2	3	4
CPU time (s)	61	35	95	68

TABLE 1. CPU time needed for the computations.

the discretization but small values (comprised between 2 and 4 degrees) are always reached. Third, at locations of stress concentration, the level-set function has peaks due to peaks of the topological gradient. Nevertheless, for a given mesh, those peaks are bounded and, as far as we have observed, they have no bad effect on the optimization process. Finally, we observe that the obtained designs depend strongly on the initialization as well as on the mesh used, even if the values of the objective function are close. However, the trivial full domain initialization provides the best and the least time consuming results, which is due to the fact the topological gradient is by nature devoted to remove matter. Starting the optimization with a rather coarse mesh tends to favor "simple" structures, which is often appreciated.

4.2. **Bridge.** This second test case is also taken from [5, 3, 4]. The working domain D is the rectangle 2×1.2 with zero vertical displacement at the bottom left and right corners. Two different loads are considered: a single load, which is a pointwise vertical unitary force applied at the middle of the bottom side, and multiple loads where three forces are applied successively (see Fig. 9). In the first situation, the Lagrange multiplier $\ell = 30$ is chosen. In the second one, the objective function is the sum of the three compliances added to the surface penalization with a Lagrange multiplier $\ell = 120$. The optimization is started on a mesh of 1985 nodes, and, after convergence, it is continued on a mesh of 7809 nodes. Figures 10 and 11 show the results obtained with the full domain initialization. As already noticed in [4], the multiple loads solution is much more realistic than the single load one.

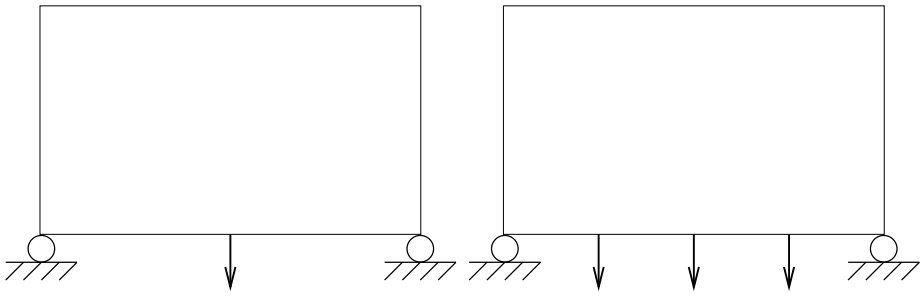

FIGURE 9. Boundary conditions for the bridge: single load case (left) and multiple loads case (right).

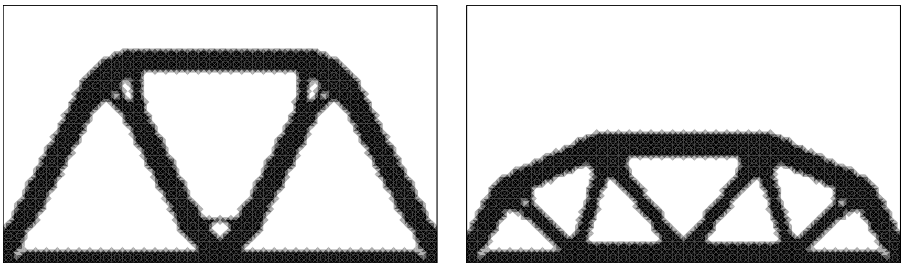

FIGURE 10. Final designs for the bridge with full domain initialization: single load case (left) and multiple loads case (right).

4.3. **Mast.** This example is taken from [3]. The working domain is T-shaped with the vertical branch of size 2×4 and the horizontal one of size 4×2. The bottom of the vertical branch is fixed and, again, we consider a single load case, with Lagrange multiplier $\ell = 15$ and a triple load case (modeling the wind effect) with $\ell = 200$. Two meshes with 2159 and 8353 nodes are handled successively. The results are depicted on Figures 12 and 13.

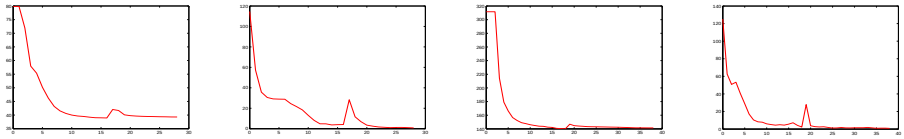

FIGURE 11. Convergences histories of the criterion $j(\Omega)$ and of the angle θ expressed in degrees for the bridge: single load case (left) and multiple loads case (right).

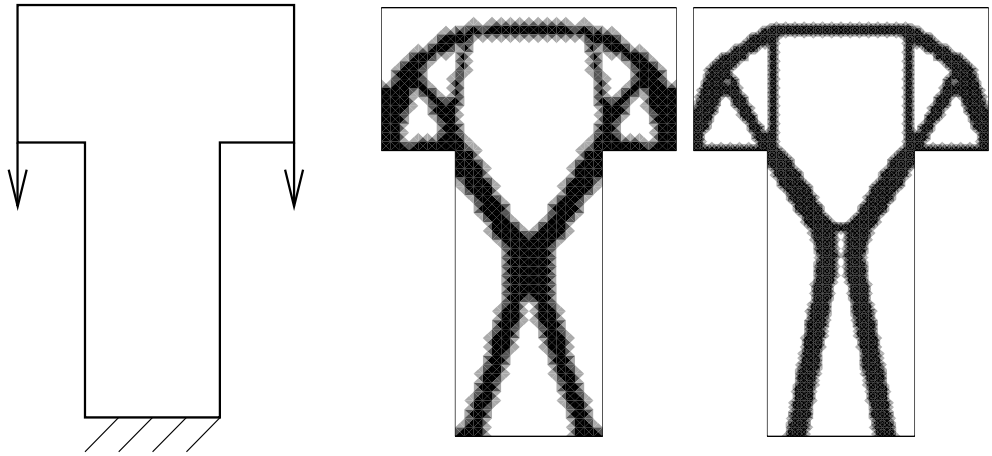

FIGURE 12. Boundary conditions and iterations 10 and 38 of the single loaded mast with full domain initialization.

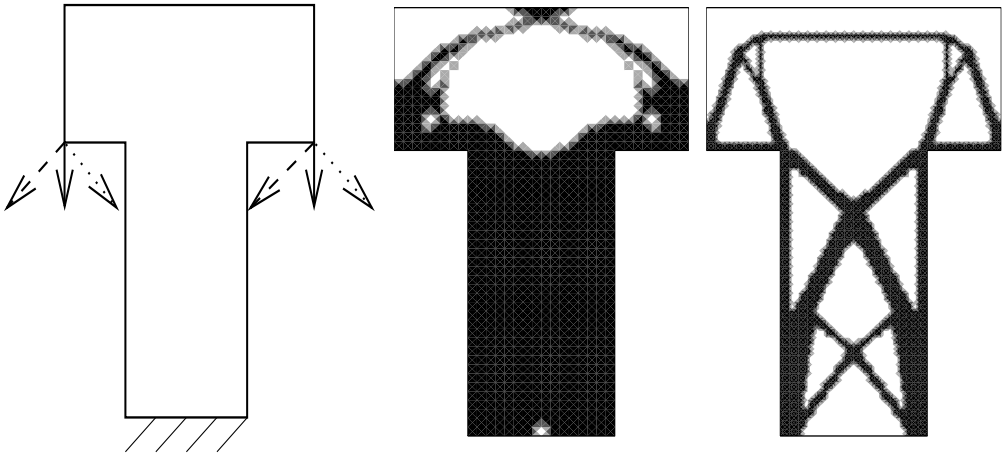

FIGURE 13. Boundary conditions and iterations 10 and 42 of the multi-loaded mast with full domain initialization.

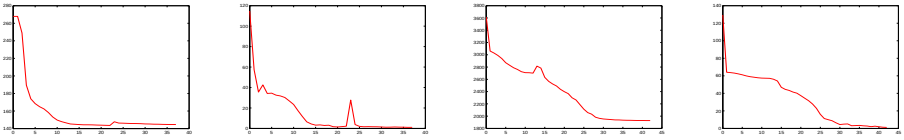

FIGURE 14. Convergences histories of the criterion $j(\Omega)$ and of the angle θ expressed in degrees for the mast: single load case (left) and multiple loads case (right).

4.4. **Gripping mechanism.** This is again a classical test case that has been treated for instance in [5, 3]. The location of the external forces is split into two regions Γ_{F1} and Γ_{F2} supporting a load φ_1 and φ_2, respectively (see Fig. 15). Free boundary conditions are prescribed elsewhere. Unlike all previous examples, we are not interested here in compliance minimization. We still consider a criterion $j(\Omega)$ of the form (3), but for the functional

$$J(u) = \beta_1 \int_{\Gamma_{F1}} \varphi_1.uds + \beta_2 \int_{\Gamma_{F2}} \varphi_2.uds,$$

with fixed coefficients β_1 and β_2. In this case, the evaluation of the topological gradient requires the solution of an adjoint problem. Figure 16 shows the results of two computations performed with the following sets of parameters: $\varphi_1 = -10n$ (n denoting the outward unit normal), $\varphi_2 = -n$, $\beta_1 = 0.1$, $\beta_2 = 1$, $\ell = 0.3$ for the first configuration (left), $\varphi_1 = -n$, $\varphi_2 = -10n$, $\beta_1 = 1$, $\beta_2 = 0.1$, $\ell = 0.3$ for the second one (right). Since thin structures are needed to obtain an efficient mechanism, we use a quite fine mesh of 8731 nodes during the whole optimization process.

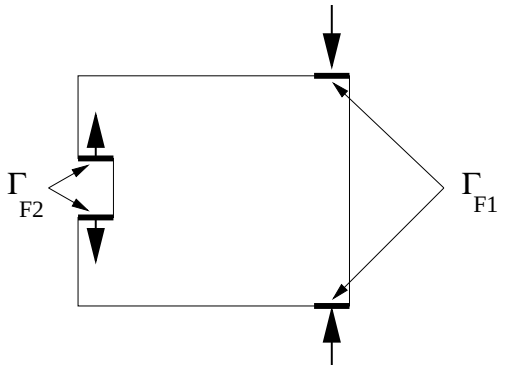

FIGURE 15. Boundary conditions for the gripping mechanism.

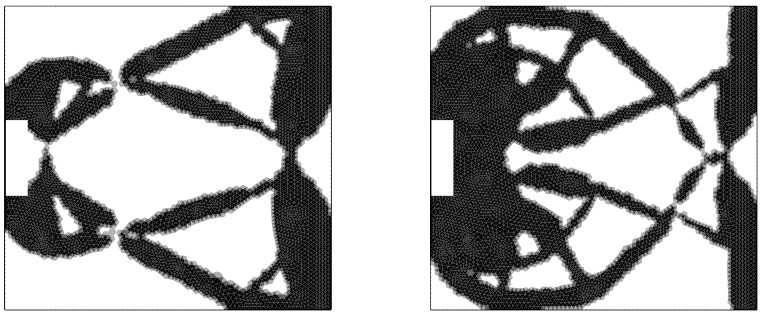

FIGURE 16. Obtained designs after 30 iterations for the gripping mechanism in two different configurations.

5. A multidisciplinary problem: optimization of a ceramic filter

5.1. **Introduction.** This problem concerns the optimal design of a certain class of waste water ceramic filters, which basically operate as follows (see Fig. 17). Thanks to an appropriate housing, the waste water is distributed all around the external surface of the filter, which has the shape of an elliptic cylinder. Due to high pressure gradients, the fluid crosses the porous medium and the filtered water reaches the top of the device through some vertical channel(s). The issue consists in determining the number, the location and the shape of these channels such

that they allow for a maximal flow rate provided that the structure does not break on the effect of the pressure.

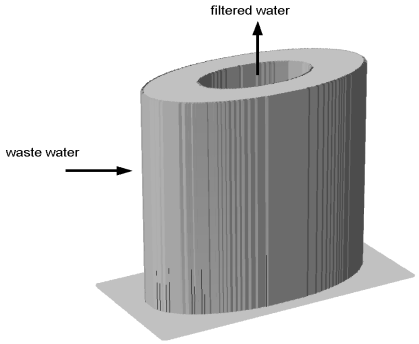

FIGURE 17. 3D geometry of the filter.

5.2. **Mathematical model.** We consider a 2D model by taking an horizontal cross-section. Therefore our computational domain D is an ellipse. To simplify the writing, since the boundary conditions on the external border are everywhere of Neumann type, we denote by Γ the boundary of D.

The behavior of the fluid is modeled by the Stokes-Brinkman system [17]:

$$\left\{\begin{array}{rcll} -\eta\Delta U_\Omega + \eta\tilde{k}^{-1}U_\Omega + \nabla p_\Omega &=& 0 & \text{in } D, \\ \text{div } U_\Omega &=& \tilde{s} & \text{in } D, \\ \eta\nabla U_\Omega.n - p_\Omega n &=& -p_{out}n & \text{on } \Gamma, \end{array}\right. \tag{18}$$

where U_Ω and p_Ω stand for the velocity and the pressure fields, p_{out} is the outside pressure, η is the dynamic viscosity of the fluid and the tilde quantities are defined by

$$\tilde{k}^{-1} = \left\{\begin{array}{lll} k^{-1} & \text{in} & \Omega, \\ 0 & \text{in} & D\setminus\overline{\Omega}, \end{array}\right. \qquad \tilde{s} = \left\{\begin{array}{lll} 0 & \text{in} & \Omega, \\ s & \text{in} & D\setminus\overline{\Omega}. \end{array}\right.$$

The letter k denotes the permeability of the porous medium and s is a sink term simulating the vertical flow. In our model, s is a prescribed negative constant.

The displacement field u_Ω of the structure is computed through the following equations, with the same notations as in (6):

$$\left\{\begin{array}{rcll} -\text{div }(\tilde{\alpha}Ae(u_\Omega)) &=& -\nabla p_\Omega & \text{in } D, \\ (Ae(u_\Omega))n - p_\Omega n &=& -p_{out}n & \text{on } \Gamma. \end{array}\right. \tag{19}$$

Since p_{out} is supposed to be constant, we remark that we obtain homogeneous boundary conditions in (18) and (19) by taking as new variable the fluctuation $p'_\Omega = p_\Omega - p_{out}$. Assuming this change of variable has been made, we consider henceforth that $p_{out} = 0$.

We still consider a criterion to be minimized $j(\Omega)$ of the form (3) with the compliance

$$J(u,p) = \int_\Gamma pu.nds - \int_D \nabla p.udx = \int_D p \text{ div } udx.$$

In our model, the additional term $\ell|\Omega|$ is a decreasing function of the flow rate, which we want to maximize. It also accounts for the price of the structure. (The material used for such filters is indeed very expensive.)

5.3. **Topological sensitivity.** The variational formulation of the b.v.p. (18), (19) reads: find $(U_\Omega, p_\Omega, u_\Omega) \in H^1(D)^2 \times L^2(D) \times H^1(D)^2$ such that

$$\left\{ \begin{array}{rcll} c_\Omega(U_\Omega, V) + d(V, p_\Omega) & = & 0 & \forall V \in (H^1(D))^2, \\ d(U_\Omega, q) & = & s_\Omega(q) & \forall q \in L^2(D), \\ a_\Omega(u_\Omega, v) & = & d(v, p_\Omega) & \forall v \in (H^1(D))^2, \end{array} \right. \tag{20}$$

with the bilinear forms

$$\begin{aligned} c_\Omega(U, V) &= \eta \int_D (\nabla U : \nabla V + \tilde{k}^{-1} U.V) dx, \\ d(V, p) &= \int_D p \text{ div } V dx, \\ a_\Omega(u, v) &= \int_D \tilde{\alpha} A e(u) : e(v) dx, \end{aligned}$$

and the linear form

$$s_\Omega(q) = \int_D \tilde{s} q dx.$$

We introduce the Lagrangian

$$\begin{array}{l} \mathcal{L}_\Omega(U, V, p, q, u, v) = \\ J(u, p) + \ell|\Omega| + c_\Omega(U, V) + d(V, p) + d(U, q) - s_\Omega(q) + a_\Omega(u, v) - d(v, p). \end{array} \tag{21}$$

Thanks to (20) it comes

$$j(\Omega) = \mathcal{L}_\Omega(U_\Omega, V, p_\Omega, q, u_\Omega, v) \qquad \forall V, q, v.$$

Although neither the Lagrangian $\mathcal{L}_\Omega$ nor the fields U_Ω, p_Ω and u_Ω are differentiable with respect to a variation of topology, the composition of the sensitivity formula as well as the relevant adjoint states can be exactly obtained by applying formally the rules of differential calculus (this statement can by proved with the help of a domain truncation technique, see *e.g.* [20]). In this setting, let us denote by $\delta_\Omega = \pm B(x_0, \rho)$ a signed domain perturbation (creation of a hole if $x_0 \in \Omega$, addition of matter if $x_0 \in D \setminus \overline{\Omega}$), and let us write the corresponding first variation of the criterion in the differential form

$$D_\Omega j(\Omega)\delta_\Omega := \tilde{g}(x_0)|B(x_0, \rho)|. \tag{22}$$

The chain rule formally applied to (21) yields :

$$\begin{array}{l} D_\Omega j(\Omega)\delta_\Omega = \partial_\Omega \mathcal{L}_\Omega(U_\Omega, V, p_\Omega, q, u_\Omega, v)\delta_\Omega + \partial_U \mathcal{L}_\Omega(U_\Omega, V, p_\Omega, q, u_\Omega, v)(D_\Omega U_\Omega \delta_\Omega) \\ + \partial_p \mathcal{L}_\Omega(U_\Omega, V, p_\Omega, q, u_\Omega, v)(D_\Omega p_\Omega \delta_\Omega) + \partial_u \mathcal{L}_\Omega(U_\Omega, V, p_\Omega, q, u_\Omega, v)(D_\Omega u_\Omega \delta_\Omega). \end{array}$$

Let us study each term successively, starting by the last one. It follows from the bilinearity of J and a_Ω that, for any δ_u,

$$\partial_u \mathcal{L}_\Omega(U_\Omega, V, p_\Omega, q, u_\Omega, v)\delta_u = J(\delta_u, p_\Omega) + a_\Omega(\delta_u, v).$$

As v is arbitrary, we choose $v = v_\Omega = -u_\Omega$ which, as a consequence of (20) together with the symmetry of a_Ω and the identity $J = d$, permits to cancel the above expression. Then we have

$$\begin{aligned} \partial_p \mathcal{L}_\Omega(U_\Omega, V, p_\Omega, q, u_\Omega, v_\Omega)\delta_p &= J(u_\Omega, \delta_p) + d(V, \delta_p) - d(v_\Omega, \delta_p) = d(2u_\Omega + V, \delta_p), \\ \partial_U \mathcal{L}_\Omega(U_\Omega, V, p_\Omega, q, u_\Omega, v_\Omega)\delta_U &= c_\Omega(\delta_U, V) + d(\delta_U, q). \end{aligned}$$

Again, the two above expressions can be canceled by an adequate choice of V and q, namely by choosing them as the solution of the adjoint problem:

$$\left\{ \begin{array}{rcll} -\eta \Delta V_\Omega + \eta \tilde{k}^{-1} V_\Omega + \nabla q_\Omega & = & 0 & \text{in } D, \\ \text{div } V_\Omega & = & -2 \text{ div } u_\Omega & \text{in } D, \\ \eta \nabla V_\Omega . n - q_\Omega n & = & 0 & \text{on } \Gamma. \end{array} \right. \tag{23}$$

Finally it remains

$$\begin{aligned} D_\Omega j(\Omega)\delta_\Omega &= \partial_\Omega \mathcal{L}_\Omega(U_\Omega, V_\Omega, p_\Omega, q_\Omega, u_\Omega, v_\Omega)\delta_\Omega \\ &= \ell \partial_\Omega |\Omega| \delta_\Omega + \partial_\Omega c_\Omega(U_\Omega, V_\Omega)\delta_\Omega - \partial_\Omega s_\Omega(q_\Omega)\delta_\Omega + \partial_\Omega a_\Omega(u_\Omega, v_\Omega)\delta_\Omega. \end{aligned}$$

The topological gradients represented by the first and the third terms come straightforwardly. The second one can be derived from [8]. The last one has been explicited in Subsection 3.1. Altogether we obtain (22) with

$$\tilde{g} = \eta \tilde{k}^{-1} U_\Omega . V_\Omega + \tilde{s} q_\Omega + \tilde{g}_{struc}(u_\Omega, v_\Omega).$$

The function $\tilde{g}_{struc}$ is given by (10).

5.4. **Numerical results.** The numerical data used are $\eta = 0.01$, $k^{-1} = 5000$ and $s = -1$. The elastic properties of the material are the same as in Section 4. A minimum thickness of ceramics on the border of the domain is imposed in order to guarantee a sufficient filtering efficiency. It corresponds to 15% of the external radius in elliptic coordinates. In the cost functional, the Lagrange multiplier $\ell = 100$ is chosen.

Figures 18, 19 and 20 show the results of two computations, corresponding to two different shapes of the working domain D. In order to avoid starting on a local extremum, the level-set function is initialized in such a way that Ω_0 is D deprived of a small elliptic hole located around its center. For those two examples, meshes of 4609 and 7073 nodes are respectively used. The slight dissymmetries on the obtained designs with respect to the main axes are entirely due to the dissymmetry of the mesh. As a postprocessing step towards the validation of these structures, we have represented the map of the highest principal stress which provides a good breaking criterion for ceramics. Indeed, the real problem is rather complicated, involving several criteria and several parameters. We have adopted a standard approach in engineering consisting in running an optimization procedure for a chosen criterion and certain fixed parameters (like the shape of the ellipse or the Lagrange multiplier). It must be checked afterwards that all constraints are satisfied by the obtained solution.

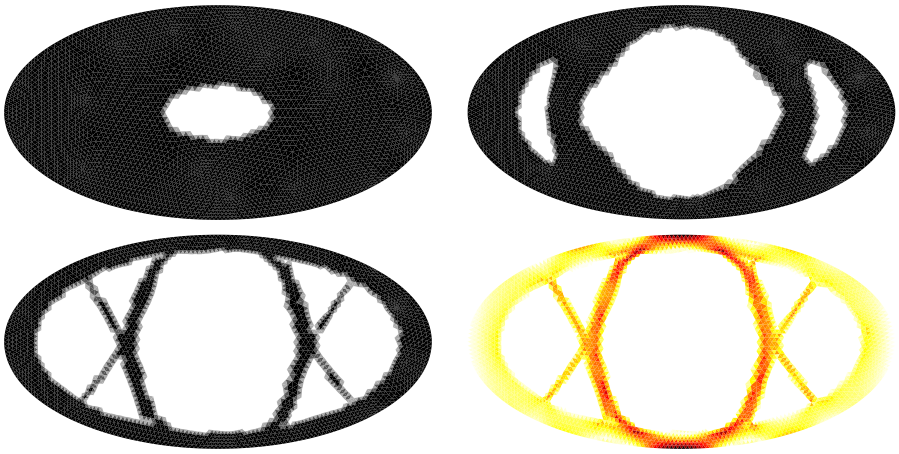

FIGURE 18. Initial guess, iterations 3 and 20 and highest principal stress of the filter with semi-axes 1×0.5.

6. CONCLUSION

We have proposed a new algorithm for simultaneous topology and shape optimization, which has the following advantages compared to other level-set based methods.

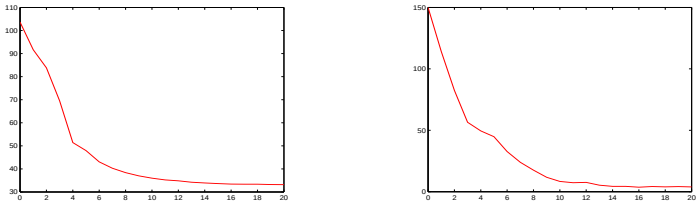

FIGURE 19. Convergences histories of the criterion $j(\Omega)$ (left) and of the angle θ expressed in degrees (right) for the filter with semi-axes 1×0.5.

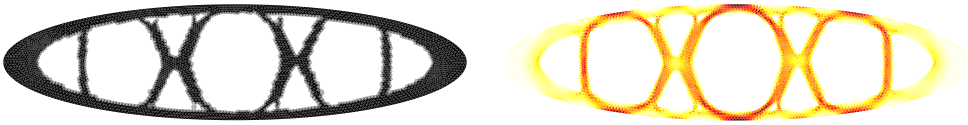

FIGURE 20. Iteration 20 of the filter with semi-axes 2×0.5: design (left) and highest principal stress (right).

- Satisfactory results are obtained without any a priori on the topology (in general, the best results are obtained with the trivial full domain initialization). For classical examples, they are very similar to the results obtained with other methods.
- The algorithm derives from an unique evolution equation which is free of arbitrary parameters.
- The level-set function has a meaning after convergence (*i.e.* at the stationary point of the evolution equation in the continuous model): It is the normalized topological gradient. Therefore the corresponding design satisfies necessary topological optimality conditions, which are even sufficient in a certain class of perturbations.
- We have used successive meshes in order to reduce the computational cost and to increase the robustness.

We point out that the accuracy as well as the efficiency could be improved by the use of a specific fast solver (see *e.g.* [25, 10]) and by an adaptive mesh refinement (see *e.g.* [29]).

However, there remain (at least) the following inconveniences. As mentioned in [3], non-relaxed topology optimization problems are generally subject to local minima and our coarse to fine mesh approach recalled above cures only partially this phenomenon. Another weakness concerns the treatment of constraints. The only one we have considered, namely a volume constraint, was handled by means of a fixed Lagrange multiplier, and so far we have no way to update it during the optimization process (its computation with the help of an outer loop, although quite costly, would be possible in this case, but this procedure would be hardly applicable to multiple constraints).

Acknowledgements. The authors are grateful to Oleg Iliev for his valuable help concerning Section 5.

REFERENCES

[1] G. ALLAIRE, *Shape optimization by the homogenization method*, Springer Verlag, New York, 2001.

[2] G. ALLAIRE, E. BONNETIER, G. FRANCFORT AND F. JOUVE, *Shape optimization by the homogenization method*, Numer. Math. 76, pp. 27-68, 1997.

[3] G. ALLAIRE, F. DE GOURNAY, F. JOUVE AND A.-M. TOADER, *Structural optimization using topological and shape sensitivity analysis via a level-set method*, Internal report no. 555, CMAP Ecole Polytechnique, 2004.

[4] G. ALLAIRE, F. JOUVE, *A level-set method for vibration and multiple loads structural optimization*, Comput. Methods Appl. Mech. Engrg. 194, pp. 3269-3290, 2005.

[5] G. Allaire, F. Jouve and A.-M. Toader, *Structural optimization using sensitivity analysis and a level-set method*, J. Comp. Phys. 194, pp. 363-393, 2004.
[6] G. Allaire and R. Kohn, *Optimal design for minimum weight and compliance in plane stress using extremal microstructures*, European Journal of Mechanics, A/Solids, 12(6), pp. 839-878, 1993.
[7] H. Ammari, H. Kang, *Reconstruction of small inhomogeneities from boundary measurements*, Lecture Notes in Mathematics 1846, Springer, 2004.
[8] S. Amstutz, *Sensitivity analysis with respect to a local perturbation of the material property*, RICAM report 2005-24.
[9] E. Bängtsson, D. Noreland and M. Berggren, *Shape optimization of an acoustic horn*, Comput. Methods Appl. Engrg. 192, pp. 1533-1871, 2003.
[10] T. Belytschko, C. Parimi, N. Moës, N. Sukumar and S. Usui, *Structured extended finite element methods for solids defined by implicit surfaces*, Intern. J. Numer. Meth. Engrg. 56, pp. 609-635, 2003.
[11] M. Bendsoe, N. Kikuchi, *Generating optimal topologies in structural design using an homogenization method*, Comput. Methods Appl. Engrg. 71, pp. 197-224, 1988.
[12] M. Bendsoe, O. Sigmund, *Topology optimization. Theory, Methods and Applications*, Springer Verlag, New York, 2003.
[13] M. Burger, *A framework for the construction of level-set methods for shape optimization and reconstruction*, Interfaces and Free Boundaries 5, pp. 301-329, 2003.
[14] M. Burger, B. Hackl and W. Ring, *Incorporating topological derivatives into level-set methods*, J. Comp. Phys. 194(1), pp. 344-362, 2004.
[15] J. Céa, S. Garreau, Ph. Guillaume, M. Masmoudi, *The shape and topological optimizations connections*, Comput. Methods Appl. Mech. Engrg. 188, pp. 713-726, 2000.
[16] S. Garreau, Ph. Guillaume, M. Masmoudi, *The topological Asymptotic for PDE systems: the elasticity case*, SIAM J. Control Optim. 39(6), pp. 1756-1778, 2001.
[17] O. Iliev and V. Laptev, *On numerical simulation of flow through oil filters*, Comput. Visual. Sci. 6, pp. 139-146, 2004.
[18] J. Jacobsen, N. Olhoff and E. Ronholt, *Generalized shape optimization of three-dimensional structures using materials with optimum microstructures*, Technical report, Institute of Mechanical Engineering, Aalborg University, 1996.
[19] C. Kane and M. Schoenauer, *Topological optimum design using genetic algorithms*, Control and Cybernetics 25, pp. 1059-1088, 1996.
[20] M. Masmoudi, *The Toplogical Asymptotic*, Computational Methods for Control Applications, R. Glowinski, H. Kawarada and J. Periaux eds., GAKUTO Internat. Ser. Math. Sci. Appl. Vol. 16, pp. 53-72, 2001.
[21] F. Murat and J. Simon, *Sur le contrôle par un domaine géométrique*, PhD thesis, Paris, 1976.
[22] S. Osher and F. Santosa, *Level-set methods for optimization problems involving geometry and constraints: frequencies of a two-density inhomogeneous drum*, J. Comp. Phys. 171, pp. 272-288, 2001.
[23] S. Osher and J.A. Sethian, *Front propagating with curvature dependent speed: algorithms based on Hamilton-Jacobi formulations*, J. Comp. Phys. 78, pp. 12-49, 1988.
[24] A. Schumacher, V.V. Kobolev and H.A. Eschenauer, *Bubble method for topology and shape optimization of structures*, Journal of structural optimization no. 8, pp. 42-51, 1994.
[25] J. Sethian and A. Wiegmann, *Structural boundary design via level-set and immersed interface method*, J. Comp. Phys. 163, pp. 489-528, 2000.
[26] O. Sigmund, *A 99 line topology optimization code written in Matlab*, Struct. Multidisc. Optim. 21, pp. 120-127, 2001.
[27] J. Sokolowski and A. Zochowski, *On the topological derivative in shape optimization*, SIAM J. Control Optim. 37, pp. 1241-1272, 1999.
[28] J. Sokolowski and J.-P. Zolesio, *Introduction to shape optimization: shape sensitivity analysis*, Springer Series in Computational Mathematics vol. 10, Springer, Berlin, 1992.
[29] R. Stainko, *An adaptive multilevel approach to the minimal compliance problem in 3D topology optimization*, Report 2004-20 of the austrian Special Research Program SFB F013.
[30] M.Y. Wang, X. Wang and D. Guo, *A level-set method for structural topology optimization*, Comput. Meth. Appl. Mech. Engrg. 192, pp. 227-246, 2003.
[31] X. Wang, M. Yulin and M.Y. Wang, *Incorporating topological derivatives into level-set methods for structural topology optimization*, Optimal shape design and modeling, T. Lewinski et al. eds, pp. 145-157, Polish Academy of Sciences, Warsaw, 2004.

Johann Radon Institute for Computational and Applied Mathematics (RICAM), Austrian Academy of Sciences, Altenbergerstrasse 69, A-4040 Linz, Austria (samuel.amstutz@oeaw.ac.at).

Fraunhofer Institut für Techno- und Wirtschaftsmathematik, Fraunhofer-Platz 1, D-67663 Kaiserslautern, Germany (andrae@itwm.fraunhofer.de).